Quantitative risk assessment of two successive landslide dams in 2018 in the Jinsha River, China

Jiangtao Yang[1,2,3], Zhenming Shi[1,2], Ming Peng[1,2]*, Hongchao Zheng[1,2], Sandra Soares-Frazão[3], Jiawen Zhou[4], Danyi Shen[1,2], Limin Zhang[5]

[1]Key Laboratory of Geotechnical & Underground Engineering of Ministry of Education, Tongji University, Shanghai 200092, China

[2]Department of Geotechnical Engineering, College of Civil Engineering, Tongji University, Shanghai 200092, China

[3]Institute of Mechanics, Materials and Civil Engineering, Université Catholique de Louvain, Louvain-la-Neuve 1348, Belgium

[4]State Key Laboratory Hydraulic & Mountain River Engineering, Sichuan University, Chengdu 610065, China

[5]Department of Civil and Environmental Engineering, The Hong Kong University of Science and Technology, Hong Kong, China

*Corresponding author: pengming@tongji.edu.cn

Abstract: Two large co-site landslide dams blocked the Jinsha River in the Sichuan Province of China in 2018. A risk analysis was carried out to quantify potential human and economic losses resulting from the failure of these dams and to investigate the influence of diversion channels on risk mitigation. Flood routing in three scenarios (i.e. after the first dam formation, after the addition of the second landslide mass on the previous one with a diversion channel, and after the occurrence of the two co-site dams without diversion channel) were simulated using HEC-RAS. The human and economic losses were evaluated using a human risk assessment model together with empirical formulations. The results show that the risk of breaching floods had increased significantly after the second co-site landslide dam formation on the pre-existing loose deposits of the first dam. This amplification effect of breaching floods was so great that the peak outflow resulting from the breaching of the second landslide dams was more important, leading to greater economic losses than those resulting from the breaching of the first dam. However, the expected loss of life caused by the breach of the two landslide dams appeared small because of the sufficient time lag provided by the long distance between the residential area and the dam site. The simulations also outline the importance of the diversion channel in decreasing the peak outflow rate and hence downstream risks. A parametric analysis on this diversion channel shows that a deep channel with a moderate longitudinal gradient can significantly decrease the peak outflow discharge at the dam site. The flood intensity and the risks at downstream towns did not change because of the relatively small attenuation rate of the peak outflow discharge. However, a smaller height of residual dam can be accessed with the use of optimal diversion channel, and then the amplification effects induced by the formation of another co-site dam in the future may be significantly reduced.

Keywords: Landslide dam, dam breaching, flood routing, quantitative risk assessment, diversion channel

1. Introduction

A landslide with a volume of 2.20×10^7 m^3 occurred at the Baige village of the Sichuan Province in China, on 10 October 2018. The rock mass moved downslope and blocked the Jinsha River, forming a 61 m high landslide dam and a 2.90×10^8 m^3 lake. The landslide dam breached with a peak outflow of 10,000 m^3/s only two days after its formation due to the large inflow rate of 1,680 m^3/s. No engineering measures, like diversion channels, could be taken to control the outburst flood because of the noticeably short time span and the remote location. Twenty-four days after the formation of the first landslide dam, on 3 November 2018, another landslide with a volume of 1.20×10^7 m^3 was deposited at the same site on top of the first landslide dam remnants. Despite the smaller volume of the landslide deposits, the second dam had a larger height (96 m) and lake volume (7.50×10^8 m^3). The time to fill up the lake was much longer than that for the first landslide dam because of a smaller inflow (which decreased to 800 m^3/s) and a larger lake volume. A diversion channel was excavated to mitigate the consequences of a potetial breaching. This allowed to reduce the lake volume to 5.24×10^8 m^3. Finally, the landslide dam was overflowed on 12 November 2018, and the outburst flood had a peak outflow rate of 33,900 m^3/s.

There have been a number of cases where successive landslide dams occured at the same site. For instance, two landslides dammed the Yigong River at the same site in Tibet, China, in 1900 and 2000 (Shang et al., 2013). The Tongkou River at Tangjiawan in China was blocked by two landslides, which were induced by the 2008 Wenchuan earthquake and a heavy rainfall event in 2016 (Fan et al., 2018; Peng et al., 2021). Similarly, the Chingshui River was repeatedly blocked at least five times by major dip slope failures during the 19th and 20th centuries in Tsaoling village, Taiwan (Tang et al., 2009). Successive landslide dam events that occur at the same site are termed as co-site landslide dams. Before the Baige landslide dams, co-site landslide dams were investigated independently, because the connection between the two closest successive landslide dams could be ignored because of the relatively long-time lag between them. However, the second Baige landslide dam was deposited on the residual materials of the first dam shortly after its breach, leading to a much larger dam height and lake volume than those of the first dam. In addition, the two co-site Baige landslide dams are closely connected because the time lag between the two successive breaches was less than a month. Thus, it was necessary to analyze the risks caused by this type of dam-breach floods and the relationship between the two co-site landslide dams. Furthermore, it is also of great significance to investigate the effect of risk mitigation measures, such as the construction of diversion channels to reduce the risks.

The existing risk assessment studies of landslide dams can be divided into qualitative and quantitative types. A qualitative risk assessment contributes to the general understanding of risks in the downstream region by ranking it based on easily accessible parameters (Ermini and Casagli, 2003; Cui et al., 2010; Yang et al., 2013; Chen et al., 2017; Frey et al., 2018) or according to the subjective ratings using fuzzy comprehensive methods (Wang and Liu, 2013; Xu et al., 2017; Liao et al., 2018). A quantitative risk assessment is used to calculate the dam breaching risk with dam failure probability and flood loss for providing a scientific basis for emergency mitigation. Peng and Zhang (2012a, b) presented a human risk assessment model (HURAM), based on Bayesian networks. Multiple parameters and their relationships are involved in this model. Peng and Zhang (2013a) developed a dynamic decision-making model by combining the dam failure probability and three types of flood losses (evacuation cost, monetized life loss and movable economic loss) using the modified HURAM. Shi et al. (2017) developed a method for efficient and quantitative risk assessment of landslide dams based on GIS technique and HURAM to produce risk maps. The method was applied to the Hongshiyan landslide dam, which was triggered by the 2014 Ludian earthquake. The existing quantitative risk assessment studies are aimed at early warning and evacuation decisions. Only the loss of life and movable property (cash, vehicles, mobile phones, etc.) are considered, since unmovable property (e.g., buildings, large furniture, and infrastructure) cannot be evacuated. However, unmovable property cannot be ignored in decision-making regarding engineering mitigation measures, such as the excavation of diversion channels and hydropower station design.

In this paper, the flood routing and risk assessments for three scenarios of Baige landslide dams (i.e. the situation after the first dam formation, the scenario after the addition of the second landslide mass on the previous one with a diversion channel, and without diversion channel) are analyzed. Also, the characteristics of the fllod wave resulting from the two successive landslide dams are investigated using HEC-RAS software and regional DEM data. Likewise, the risks of life and property loss are assessed based on the HURAM and a group of empirical equations. The amplification effect of co-site landslide dam breach and the optimal design strategy of the diversion channel are also discussed.

2. Characteristics of the Baige landslide dams

The Jinsha River is a tributary of the Yangtze River in its upper reach and flows through Tibet, Sichuan and Yunnan Provinces. Due to the upheaval of the Tibetan Plateau, this region features pronounced tectonic structures, including a series of NW-trending folds and faults. The rocks consist of phyllite, argillaceous slate, fragmented sandstone, marble and gneiss mainly, are highly fractured, thereby providing abundant material resources for mass movements. In addition, deep erosion by the Jinsha River steepens the hillslope. Consequently, the upstream reach of Jinsha River District has become a site of frequent geological disasters, including landslides, rock avalanches and debris flows. Li et al. (2006) recorded more than 339 slides and falls along the Jinsha River, out of which 61 ancient failures blocked the river channel (Xiong et al., 2020).

The two successive landslides analyzed here are positioned in the upper reach of the Jinsha

River at the Baige village (98°42′17″E, 31°04′59″N), and 52 km downstream from the Jiangda County of the Sichuan Province (Fig. 1). The landslides formed on the right bank of the valley with a hillslope of 50° to 60°. The landslide crowns are positioned at altitudes of 2,880 m to 3,720 m, whereas the riverbed is at 2,870 m (Fig. 2). The landslides occurred on serpentinite and Proterozoic gneiss, where the V-shaped valley is about 150 m wide (Fan et al., 2019).

Fig. 1 Jinsha River and the two successive Baige landslide dams: (a) location of the landslide dams; (b) first dam; (c) second dam. Source: Modified from the figures published by the Hydrology and Water Resources Survey Bureau of Sichuan Province.

2.1. First landslide

The first Baige landslide occurred at 22:00 on 10 October 2018. The stability of the slope was influenced by a series of NW-striking faults and long-term rainfall infiltration. The rocks had lost their strength owning to the long-term movement on faults, wide-open joints and deep weathering. The rockslide began long before 2018 with a slow creep along a fracture at the interface of different rock layers, and then the crack propagated under the action of gravity and it gradually cut through the slope surface. The landslide can be divided into the upper and lower parts (Fig. 2). At first the rock mass from the lower part of the slope moved with a relatively high velocity and was finally deposited in the valley damming the Jinsha River (Fig. 3). Then the rock mass constituting the upper part failed just after the loss of the support from the lower part and moved toward the opposite bank. In this process, it collided with the mass from lower part and was eventually deposited on the right bank near the river (Ouyang et al., 2019; Shen et al., 2020).

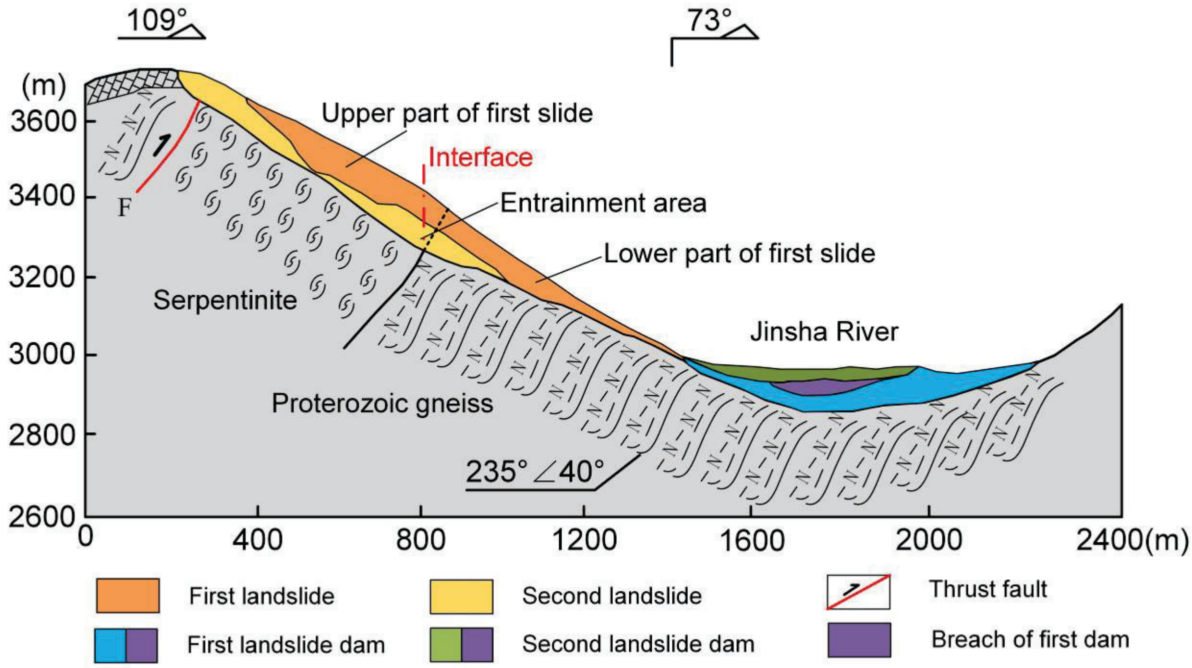

Fig. 2 Geological cross-section of two Baige landslides and dams (downstream view). Source: Modified from Xu et al. (2018).

The first Baige landslide had a volume of about 2.50×10^7 m^3 and its main sliding direction was 90°E (Fig. 2). The parameters of the slide deposit and its formed barrier lake are listed in Table 1.

Table 1 Dimensions of two Baige landslide and the dams.

Landslide	Landslide volume(m^3)	Height (m)	Crest width(m)	Lake volume(m^3)	Dam volume(m^3)	Inflow rate(m^3/s)
First	2.50×10^7	61	300	2.90×10^8	2.40×10^7	1,680
Second	1.20×10^7	96	79.4	7.50×10^8	3.02×10^7	800

2.2. Second landslide

The second landslide occurred at 17:40 on 3 November 2018 (24 days after the formation of the first dam). The slide developed on a weak serpentinite bank mainly, which was severely fragmented by a thrust fault, and it also had wide cracks induced by the first failure. The slide was triggered by rainfall infiltration and long-term creep (Fan et al., 2019). During downwards movement, the second slide collided with and scraped the residual material from the first landslide on the right bank near the river, and was finally deposited in the river channel (Fig. 3).

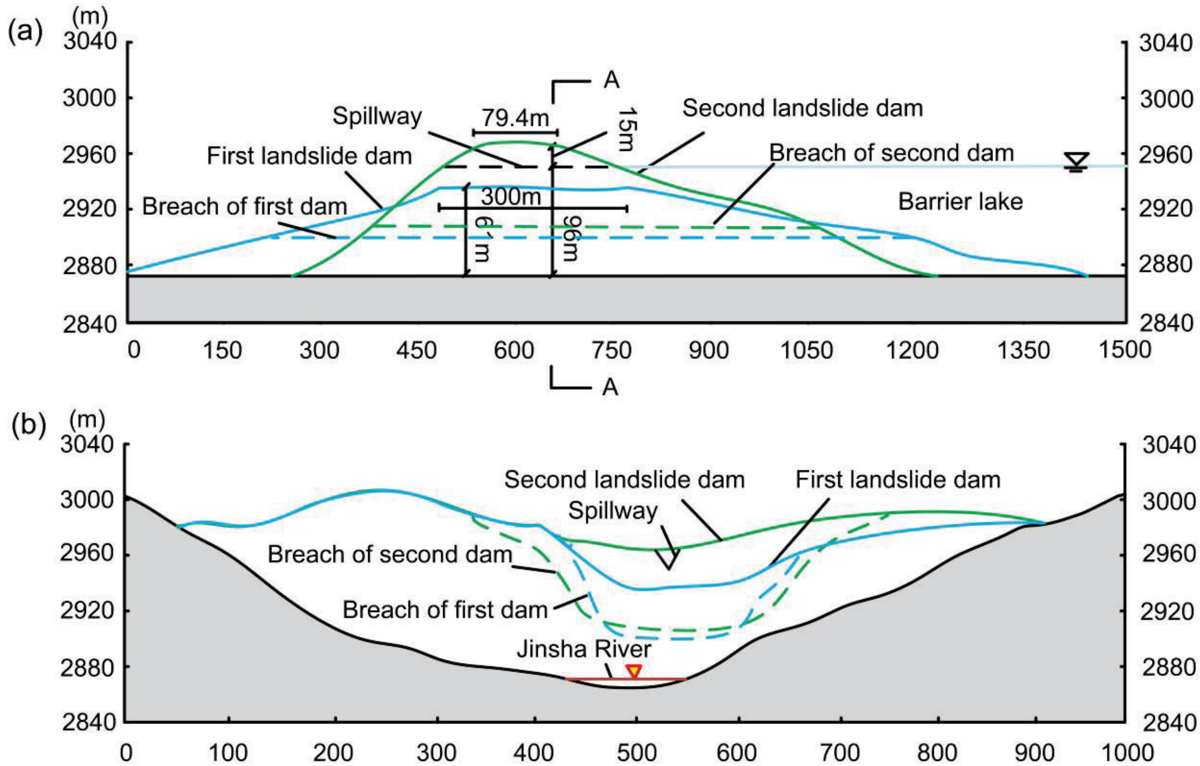

Fig. 3 Cross sections of the two Baige landslide dams: (a) along the river; (b) across the river, along A-A.

The second landslide had a total volume of 1.20×10^7 m^3, out of which the rock detached from 3,000 to 3,800 m altitude contributed 3.50×10^6 m^3 and the entrained from the previous landslide provided 8.50×10^6 m^3 of debris (Fan et al., 2019; Ouyang et al., 2019). The landslide further blocked the Jinsha River and increased the average thickness of the deposit by about 30 m compared to the first landslide dam. The new landslide dam was 96 m high, with a crest width of 79.4 m. The dam had a total volume of 3.02×10^7 m^3, and formed a large lake behind it with a volume of 7.50×10^8 m^3 (Table 1). Thus, despite a lesser landslide volume, the second landslide blocked the river with a larger dam height and lake volume.

2.3. First landslide dam: timeline and emergency mitigation measures

The timeline and relevant emergency mitigation measures taken for first Baige landslide dam are shown in Fig. 4. After the formation of the first landslide dam, the water level rose quickly because of the large inflow rate (1,680 m^3/s). Several villages were gradually inundated, forcing more than 10,000 people to evacuate from their homes by 16:00 on 11 October. At least 11,500 people in Yunnan Province were evacuated before 12 October, and five hydropower stations downstream with a total reservoir water supply of 5.23×10^8 m^3 were discharged to cope with the flood. The water level increased to 2,931 m resulting in a lake volume of 2.20×10^8 m^3 when it began to overflow the dam crest at 17:30 on 12 October. The lake volume increased continuously until reaching its maximum capacity of 2.90×10^8 m^3, and the dam failed by overflowing at 0:45 on 13 October. A peak outflow rate of 10,000 m^3/s was observed at 7:00 on 13 October, and the peak discharges observed at the two hydrological monitoring stations (HMSs) downstream were 7,800 m^3/s at the Yebatan HMS at 8:00 on 13 October (70 km downstream of the dam site) and 7,060 m^3/s at the Batang HMS at 20:00 on 13 October (190 km downstream of the dam site). The outburst flood flowed through Yunnan Province on 14 October. The first landslide dam stopped overflowing at 14:00 on 14 October, and the outflow rate remained in balance with the inflow rate. Approximately 3.00×10^6 m^3 of dam material was washed away, eventually forming a breach with a depth of 32 m, a bottom width of 80 m and a top width of 180 m (Zhang et al., 2019). The peak outflow rates at both the dam site and two hydropower stations downstream are shown in Table 2.

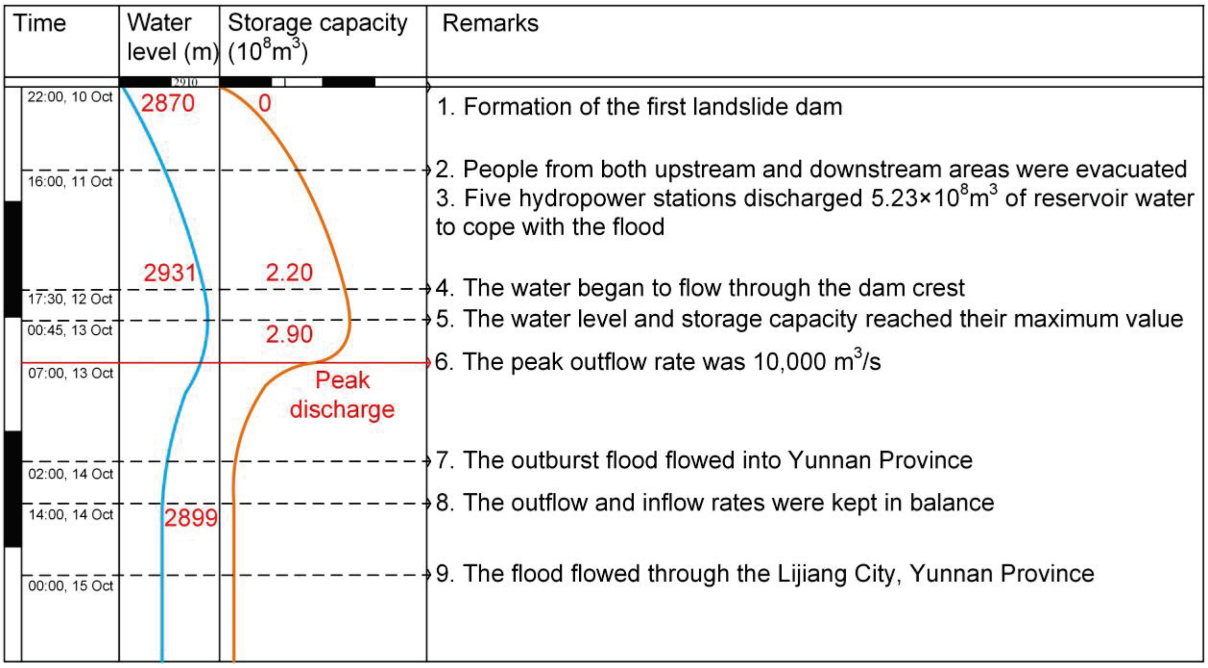

Fig. 4 Timeline of the first landslide dam formation, its outburst flow, and applied emergency measures.

2.4. Second landslide dam: timeline and emergency mitigation measures

The timeline and emergency mitigation measures applied to the second landslide dam are shown in Fig. 5. The inflow rate was reduced from 1,680 m^3/s to 800 m^3/s, compared to the time of the first dam which allowed for a longer time for mitigation measures before the dam breach. More than 25,000 people both upstream and downstream were evacuated before 9 November. Five reservoirs downstream were emptied before the dam breached, and a man-made coffer under construction, which was almost overtopped by the flood caused by the breach of the first landslide dam, was partially dismantled on 9 November (Zhang et al., 2019). To reduce the lake volume and the corresponding risk caused by the outburst flood, a diversion channel with a depth of 15 m, a top width of 42 m and a bottom width of 3 m was excavated at the dam crest at 20:00 on 10 November. The water level and lake volume continuously increased to 2,952 m and $5.24×10^8$ m^3, respectively, when the water began to flow through the diversion channel at 10:50 on 12 November (9 days after its formation). The peak outflow rate at the dam site of the second landslide dam was 33,900 m^3/s at 15:00 on 13 November. The outburst flood reached Lijiang City (550 km downstream) at 21:00 on 14 November and submerged a large amount of farmland and buildings. The outburst flood from the second landslide dam abated at 8:00 on 15 November, forming a breach with a depth of 61 m, a top width of 300 m and a bottom width of 90 m (Zhang et al., 2019). The peak outflow rate and maximum water level observed at the four HMSs downstream are shown in Table 2.

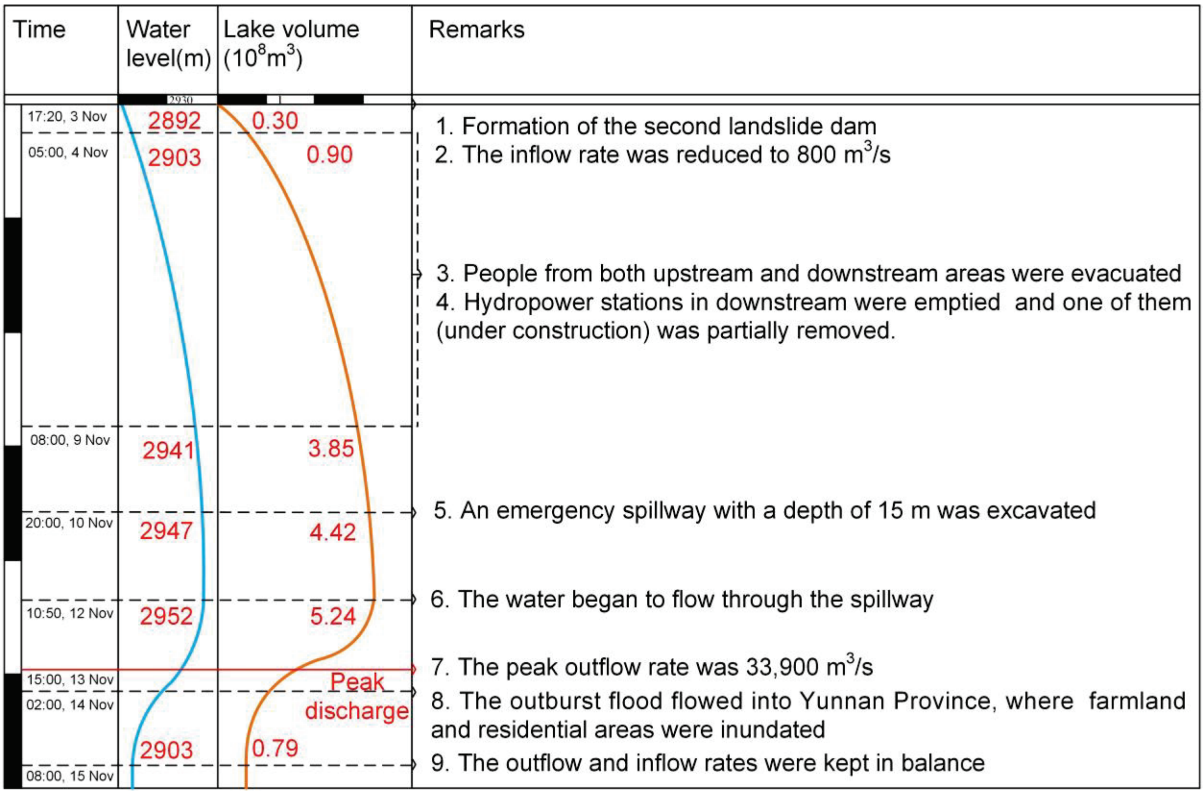

Fig. 5 Timeline of the second landslide dam formation, its outburst flow, and applied emergency measures.

2.5. Observed damages in the downstream area

The outburst flood of the two Baige landslide dams impacted almost 800 km (from the dam site to Mingyin town in the Yunnan Province) of the dowmstream region (Fig. 6). More than 10 towns (such as Benzilan, Judian and Shigu) in the Yunnan Province adjacent to the Jinsha River were affected by outburst floods, which submerged many residential areas and a large part of farmland. Out of these towns and villages, six locations in five towns of the Yulong County were severely damaged by the outburst flood. As reported by the local government, approximately 18,000 people were evacuated before the dam breach. The flood submerged a large number of buildings and extensive farmland in the Yulong County and also damaged many road, hydropower stations, bridges, and pipelines (Zhang et al., 2020). The total economic loss in the Yulong County was estimated at 4.20 billion yuan.

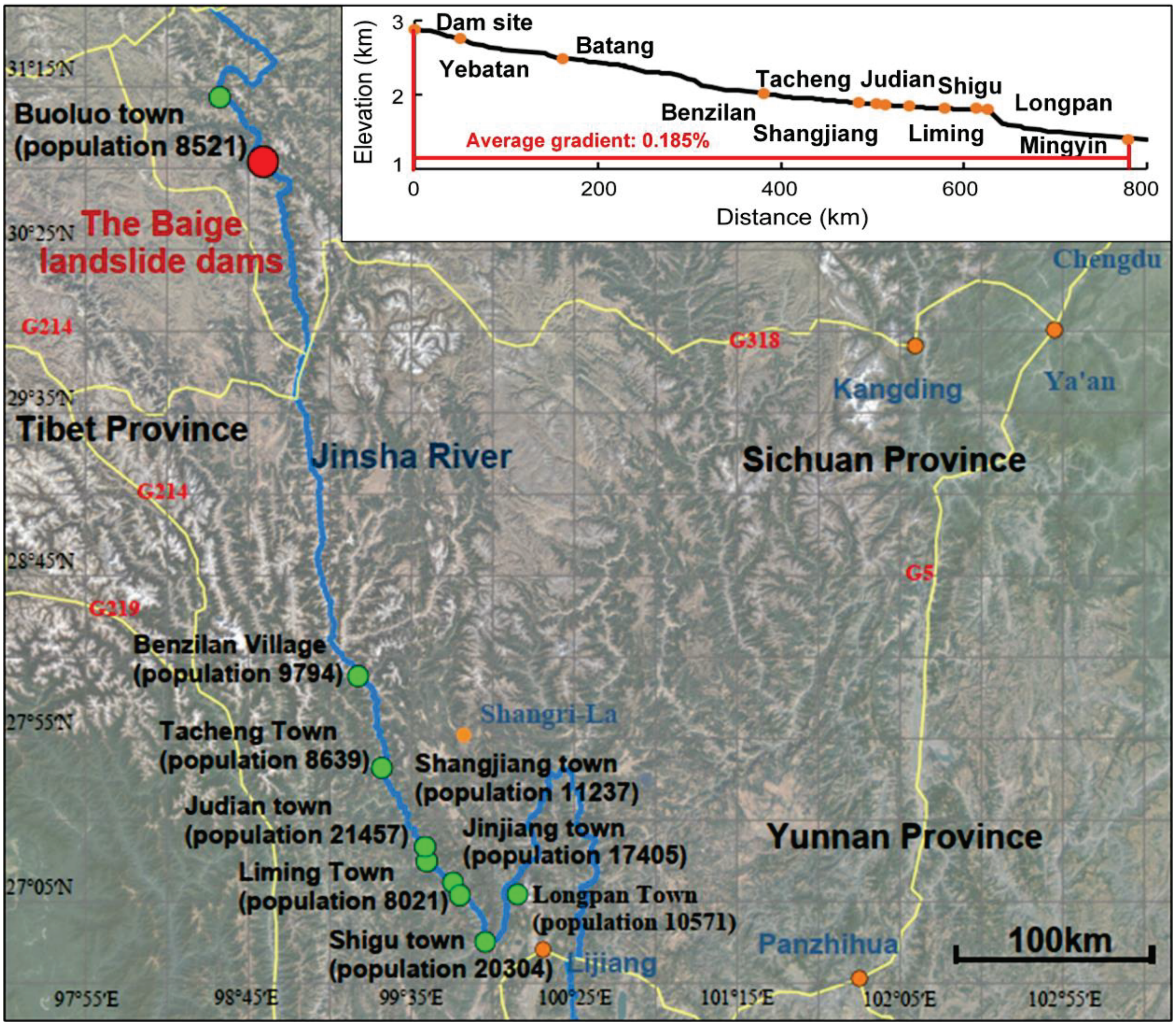

Fig. 6 Potential flooded areas caused by the breach of two landslide dams.

Table 2 Measurements during the breach of two Baige landslide dams.

Landslide dam	HMS	Measured data			
		Distance (km)	Maximum water level (m)	Peak outflow rate (m^3/s)	Time to peak outflow rate (h)
First	Dam site	0	–	10,000	5:30 AM 13 Oct
	Yebatan	70	–	7,800	8:00 AM 13 Oct
	Batang	190	–	7,060	8:00 PM 13 Oct
Second	Dam site	0	–	33,900	6:00 PM 13 Nov
	Batang	190	2494.91	20,900	2:00 AM 14 Nov
	Benzilan	382	2018.98	15,700	1:00 PM 14 Nov
	Tacheng	487	1895.12	12,200	8:00 PM 14 Nov

Shigu	574	1826.47	7,170	9:00 AM 15 Nov

3. Flood routing analysis

To analyze the characteristics of the outburst flood caused by the breach of the two Baige landslide dams and the inundation downstream, three different scenarios are considered (Table 3), including the first landslide dam (Scenario 1), the second landslide dam with a diverion channel (Scenario 2) and without a diversion channel (Scenario 3). A larger lake volume (7.24×10^8 m^3) and water level (96 m) had to be considered in Scenario 3 due to the absence of the diversion channel.

Table 3 Simulation scenarios and their basic features.

Scenario	Dam geometrical feature			Lake volume (m^3)	Inflow rate (m^3/s)	Spillway feature		
	Height (m)	Length (m)	Width (m)			Top width(m)	Bottom width(m)	Depth (m)
S1	61	200	300	2.20×10^8	1680	–	–	–
S2	96	200	79.4	5.24×10^8	800	42	3	15
S3	96	200	79.4	7.24×10^8	800	–	–	–

Table 4 shows the breach parameters of the three scenarios obtained from the field records and numerical results (Zhang et al., 2019), and these data is used to calibrate the outflow curve used in flood routing simulation. The recorded breach size and duration are used in Scenarios 1 and 2 for dam breaching and flood routing simulation, while the values obtained from numerical simulation are applied for Scenario 3 due to the absence of measured data.

Table 4 Breach parameters of three scenarios. The numerical results are from Zhang et al. (2019).

Scenario		Breach size (m)			Peak outflow rate (m^3/s)	Breach duration (h)
		Depth	Top width	Bottom width		
S1	Measured data	32.0	180.0	80.0	10,000	21.0
S2	Measured data	61.0	300.0	90.0	33,900	51.2
S3	Numerical data	66.1	414.8	225.9	55,579	45.0

Flood routing for the three scenarios was simulated using the one-dimensional river hydraulics analysis program HEC-RAS (HEC, 2008). The river channel model established in

HEC-RAS is shown in Fig. 7a. The model is composed of 265 river channel profiles, which were obtained from regional DEM data (Google Map, 2018). A total of 16,752 profiles were interpolated with a maximum elevation difference of 0.1 m to ensure computational stability. The relationship between the water level and storage capacity used in the flood analysis is shown in Fig. 7b, and the Manning coefficients for the riverbed and floodplain of the Jinsha River are 0.03 and 0.05 according to the manual of HEC-RAS (HEC, 2008). The dam models in the three different scenarios are shown in Fig. 7c, in which the dotted line refers to the final breach size according to the recorded data (Table 4).

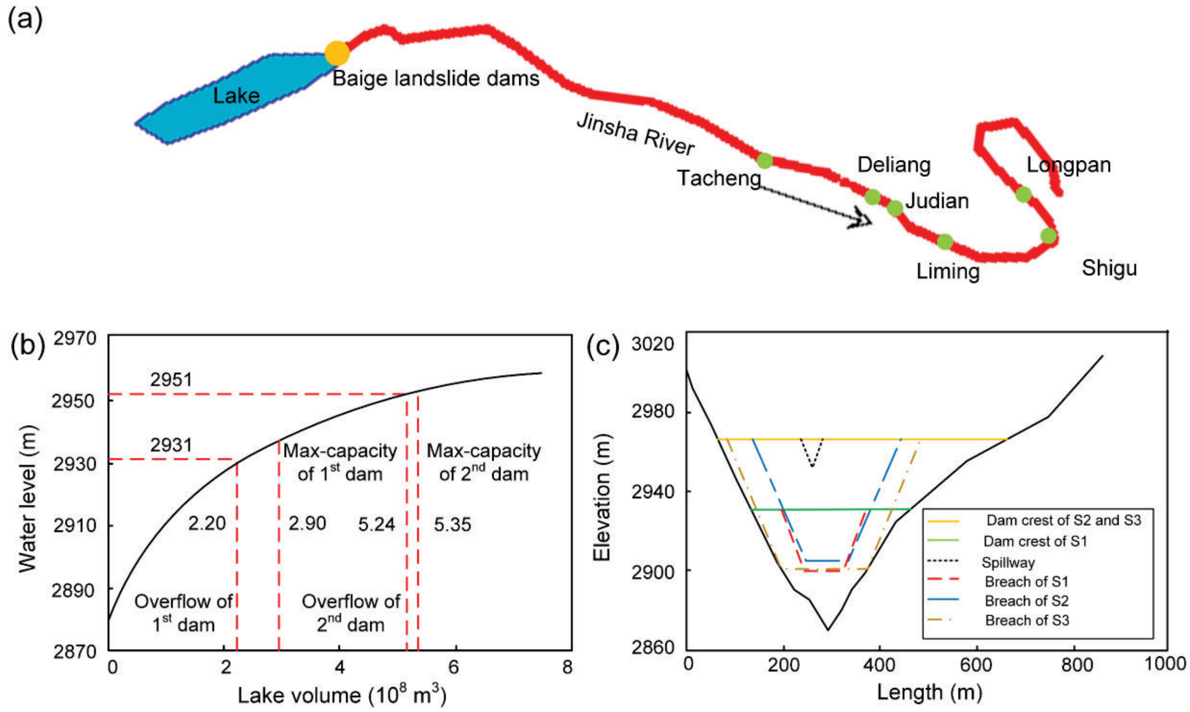

Fig. 7 Input data of numerical model: (a) river channel model established in HEC-RAS; (b) the relationship between water level and the storage capacity; (c) dam model and the final breach of three scenarios.

3.1. Scenario 1

Fig. 8a shows the outflow rate for Scenario 1, which closely corresponds to the recorded values at the dam site as well as at Yebatan and Batang HMSs. The largest peak outflow rate at the dam site is 10,551 m^3/s, and it decreases downstream. Various hydraulic parameters, including the peak outflow rate, flow velocity and maximum water depth, are recorded at six locations from five towns (two locations in Judian town) in the Yulong County, Yunnan Province, as shown in Table 5. The flood flows through these locations with no severe impact on residents and infrastructures in local area.

Based on the maximum water depth, regional DEM data, pictures and videos taken from the affected area, the extent of inundation at six locations downstream of Scenario 1 are shown in Fig. 9. There is no inundated residential area or farmland during the event related to the breach of the first Baige landslide dam in the six locations, except in Judian town. The only inundated area in Judian town is farmland with an area of 0.01 km^2 (Table 6). No engineering mitigation needs to be considered before the breach of the first landslide dam.

3.2. Scenario 2

Due to the smaller inflow rate (i.e., 800 m^3/s) and larger volume available, a longer time period is required for Scenario 2 to fill up the lake. The outflow rate at the dam site reaches its peak 25 hours after the water begins to flow through the diversion channel (Fig. 8b). The peak outflow rate at the dam site for Scenario 2 is 33,969 m^3/s, which is more than three times the peak outflow for Scenario 1. The flood from Scenario 2 impacts the towns and villages downstream much more severely than in Scenario 1. As shown in Table 5, the peak outflow rates increase significantly due to the higher dam height and larger lake capacity of the second Baige landslide dam. In Tacheng, Deliang, Judian and Liming, the peak outflow rates are more than 7,000 m^3/s higher than those in Scenario 1. The peak outflow rates in the other two locations (i.e. Shigu and Longpan) also increase 3,000 m^3/s. In addition, the attenuation of the peak outflow rate in Scenario 2 is also faster than that in Scenario 1 (Fig. 8d). This is because the attenuation of the peak outflow rate is sensitive to the size and shape of the flood hydrograph, and a larger peak outflow rate and a ‘slenderer’ hydrograph occur in Scenario 2, leading to more energy loss caused by the resistance of the riverbed and floodplain.

The inundation area in Scenario 2 is much larger than that in Scenario 1, as shown in Fig.

9. All six locations downstream are inundated due to the increased flood intensity. As in Deliang village, about 0.19 km^2 of the residential area is inundated, with an at-risk population of 1,038. The situations in Judian and Shigu towns are very severe, where the floods inundate 0.97 km^2 and 0.31 km^2 residential area of these two towns respectively. The populations at risk in these two towns are estimated to 5,303 and 1,700. Due to the high altitudes of Tacheng, Liming and Longpan towns, the inundated residential areas in these three locations are relatively small, with values of 0.04 km^2, 0.06 km^2 and 0.01 km^2 and at-risk populations of 150, 181 and 30, respectively. The total inundated farmland area of S2 in Yulong County is estimated at 11.69 km^2 (Table 6).

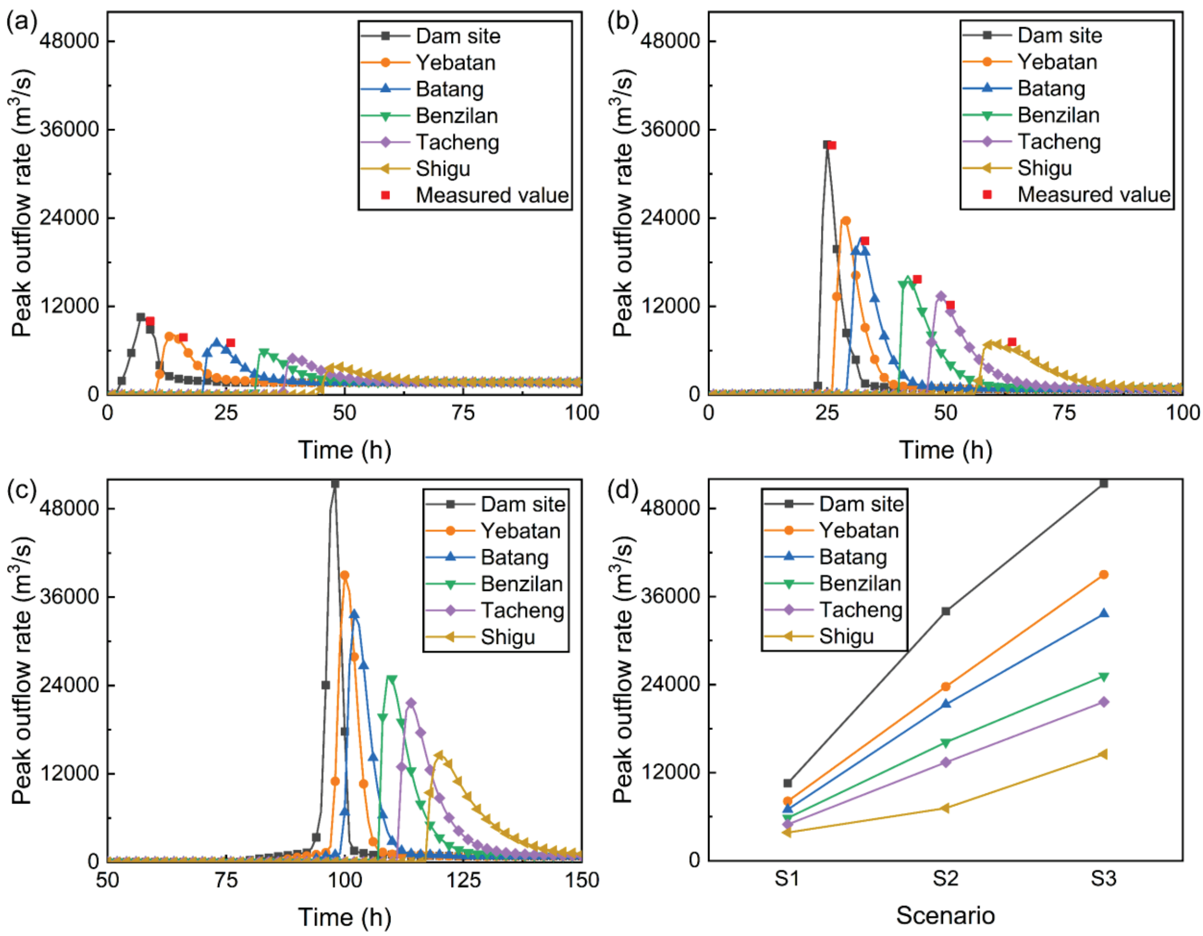

Fig. 8 The calculated discharge in three scenarios: (a) S1; (b) S2; (c) S3; (d) variation of peak outflow rate.

3.3. Scenario 3

In Scenario 3, the flood is severely enhanced by the absence of diversion channel (Fig.

8c). Compared with Scenario 2, it takes an extra 70 hours to reach the peak outflow rate of 51,394 m^3/s, which is 1.5 times the peak outflow rate in Scenario 2. The peak outflow rates in the six downstream locations also increase significantly (Table 5). In Tacheng and Deliang, the peak outflow rates are more than 8,000 m^3/s higher than those in Scenario 2. The flood intensity decreases downstream, and peak outflow rates of Judian, Liming and Shigu in Scenario 3 are approximately 6,000 m^3/s higher than those in Scenario 2, while only 3,619 m^3/s increment can be accessed in Longpan. In addition, because a larger peak outflow rate occurs in Scenario 3, the attenuation of the peak outflow rate in Scenario 3 is also faster than that in Scenario 2, as shown in Fig. 8d. The maximum water depth and flow velocity on the floodplain of six locations also increase significantly (Table 5). The most severe floods occur in Deliang, Judian and Shigu, with maximum water depths of 7.13 m, 10.65 m and 8.71 m, respectively. The maximum water depths in the other three locations (Tacheng, Liming and Longpan) are relatively small, while the rate of increase is larger than that in Deliang, Judian and Shigu due to the high and steep terrain in these locations.

Table 5 Peak outflow rate Q_p (m^3/s), maximum depth of inundation W_{dm} (m), and flow velocity on the flood plain V (m/s) at various stations from Yulong County.

Station	Hydraulic parameter	Scenarios S1	S2	S3
Dam site	Q_p	10,551	33,969	51,394
Tacheng	Q_p	4,947	13,406	21,651
	W_{dm}	0	1.52	5.47
	V	0	2.56	2.99
Deliang	Q_p	4,905	13,188	21,424
	W_{dm}	0.56	5.43	7.13
	V	0.92	1.86	2.55
Judian	Q_p	4,672	11,873	18,266
	W_{dm}	2.63	7.47	10.65
	V	0.45	1.06	1.13
Liming	Q_p	4,533	11,552	17,902
	W_{dm}	0	1.49	4.96
	V	0	1.47	1.89
Shigu	Q_p	3,846	8,844	14,516
	W_{dm}	0	4.52	8.71
	V	0	0.30	0.44
Longpan	Q_p	2,652	6,543	10,162

	W_{dm}	0	0.56	4.35
	V	0	0.95	1.25

Table 6 Various inundation scenarios for Yulong County. A_R: residential area, A_F: farmland.

Location	Inundated area					
	S1		S2		S3	
	A_R (km^2)	A_F (km^2)	A_R (km^2)	A_F (km^2)	A_R (km^2)	A_F (km^2)
Tacheng	–	–	0.04	0.81	0.12	1.19
Deliang	–	–	0.19	0.89	0.19	1.08
Judian	–	0.01	0.97	4.91	1.36	6.05
Liming	–	–	0.06	0.95	0.15	1.30
Shigu	–	–	0.31	3.24	0.61	4.33
Longpan	–	–	0.01	0.89	0.03	1.16
Sum	–	0.01	1.55	11.69	2.42	15.11

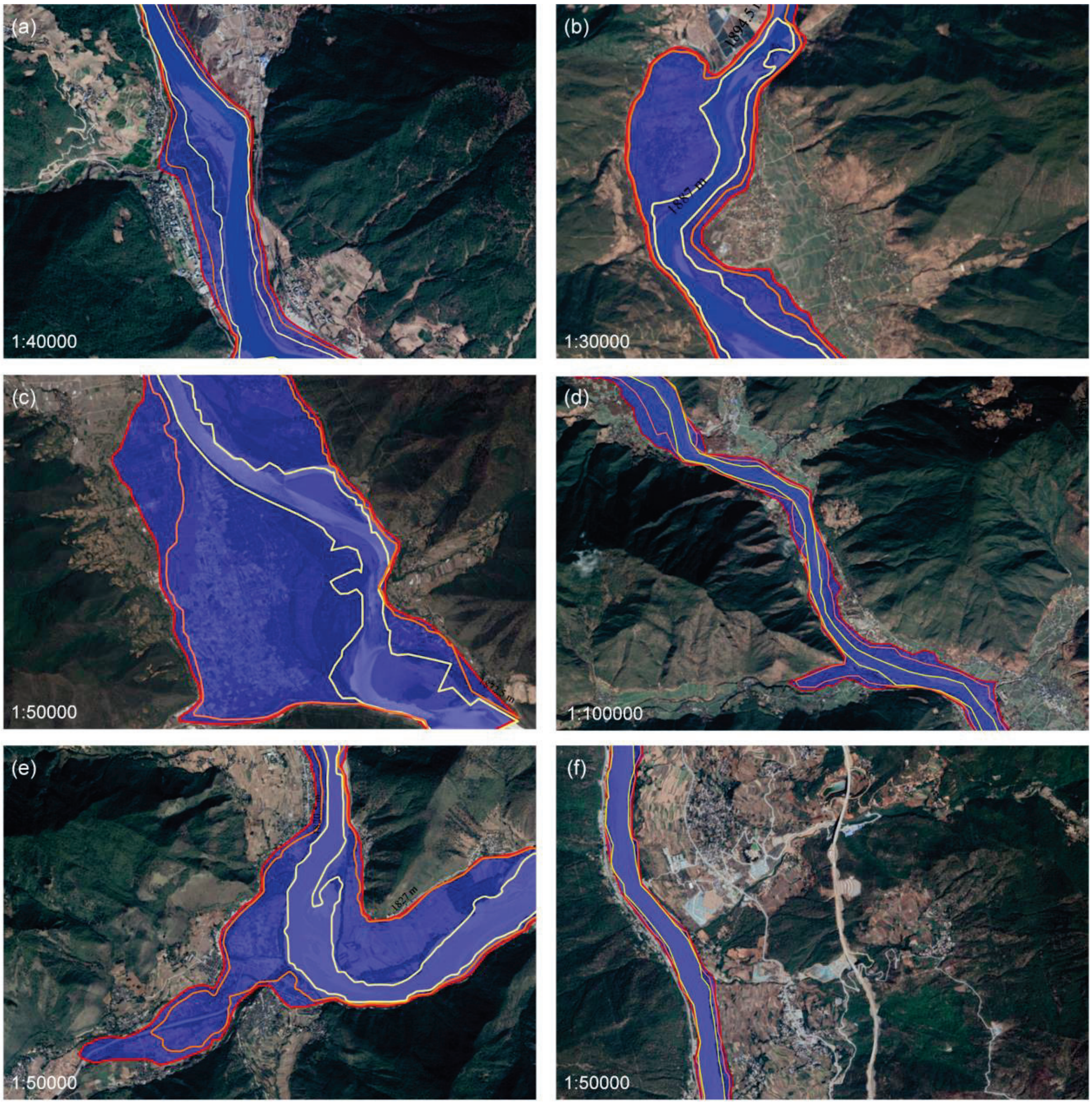

Fig. 9 Inundation area in six locations of Yulong County with three scenarios. (a) Tacheng; (b)

Deliang; (c) Judian; (d) Liming; (e) Shigu; (f) Longpan (S1 -Yellow line, S2 – Orange line and S3 – Red line).

Due to the enhanced flood intensity, both the inundated residential and farmland areas increase, as shown in Fig. 9. Compared with the difference in the inundated area between S1 and S2, the difference between S2 and S3 is relatively small in Deliang and Judian, with inundated residential areas of 0.19 km^2 and 1.36 km^2, respectively. This is because these two locations are located at the alluvial-proluvial fan along the river, which is already almost totally submerged in S2, leading to a small difference in these locations. The difference in the inundated residential area increases significantly in Tacheng, Liming and Longpan compared to the difference between S1 and S2, while the total inundated residential areas in these three locations are relatively small, with values of 0.12 km^2, 0.15 km^2 and 0.03 km^2, respectively. The maximum difference in the inundated residential area (0.30 km^2) occurs in Judian town, with a total inundated residential area of 0.61 km^2. The at-risk populations are estimated to 450, 1,038, 7,362, 452, 3,345 and 92 in these six locations. The total inundated farmland area in S3 is 15.11 km^2, which is 3.42 km^2 larger than that in S2, as shown in Table 6.

4. Human risk assessment

The risk faced by humans caused by dam-break floods can be calculated as:

$$\mathrm{LOL} = \sum PAR_i \times F_i \tag{1}$$

where LOL refers to the loss of life, F_i is the fatality ratio in subarea *i*, and PAR_i is the at-risk population in subarea *i*, which is estimated by the inundated residential area. Thus, the loss of life can be obtained only if the fatality ratio can be calculated. Therefore, the HURAM model (Peng and Zhang 2012b) was applied to calculate the fatality ratio.

A specific HURAM model diagram is shown in Fig. 10. The model was established from 15 nodes with discrete states and 23 arcs based on a Bayesian network. The prior (conditional) probabilities were quantified with statistical data, empirical equations, and physical analysis. The model works to obtain the evacuation and fatality rates by updating the prior probabilities.

The fatality ratio can be estimated once the eight basic nodes are quantified, including the evacuation distance, time of day, distance to dam site, number of stories in a building, dam breach duration, water depth, flow velocity and building type. Among these nodes, the evacuation distance and water depth are set as variables according to the flood routing results. For this purpose, the evacuation distance is divided into different intervals as 0-100 m, 100-500 m, 500-2,000 m, and >2,000 m and the water depth is classified into 0-1.5 m, 1.5-3 m, 3-4.5 m, 4.5-6 m, 6-7.5 m, 7.5-9 m and >9 m intervals. The other six nodes remain constant and can be quantified by flood routing results and field observations.

The buildings are assumed to be three-storied concrete-brick structures. The risk zoning map of the inundated area in each town or village can be obtained based on the evacuation distance and the water depth (Fig. 11), where the risks levels are shown in various colors. The extent of inundation in different colors as well as its percentage in terms of the total inundation area is calculated to estimate the evacuation rate and fatality ratio. Finally, the loss of life can be obtained from the model.

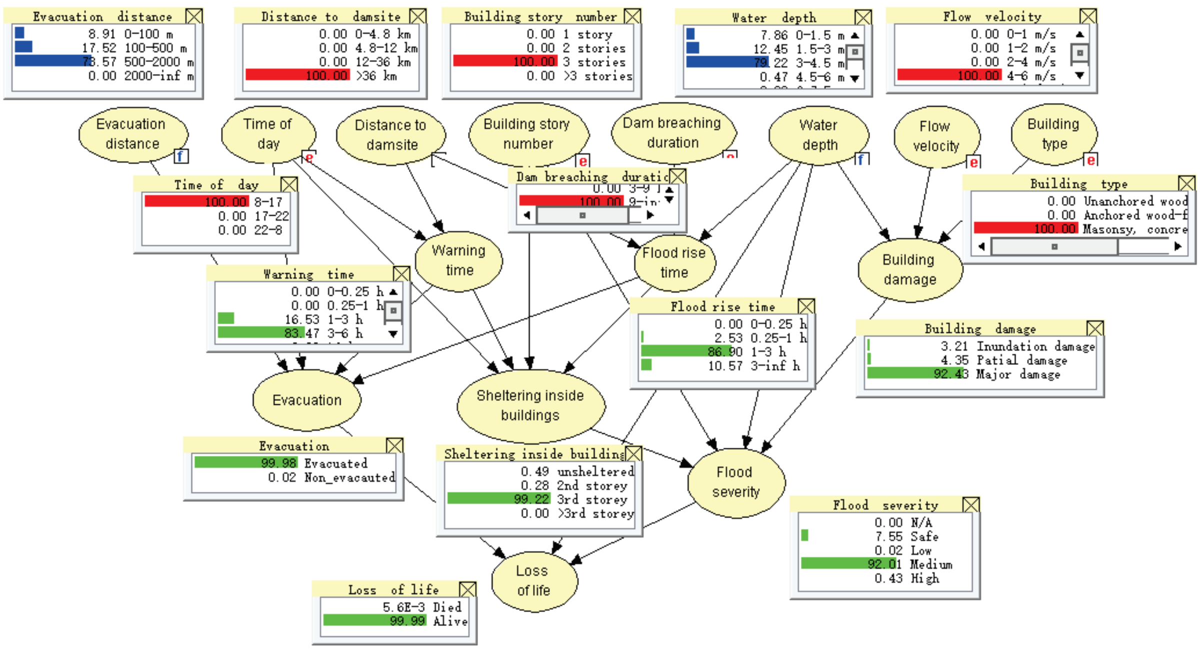

Fig. 10 The application of HURAM for the Judian town as an example.

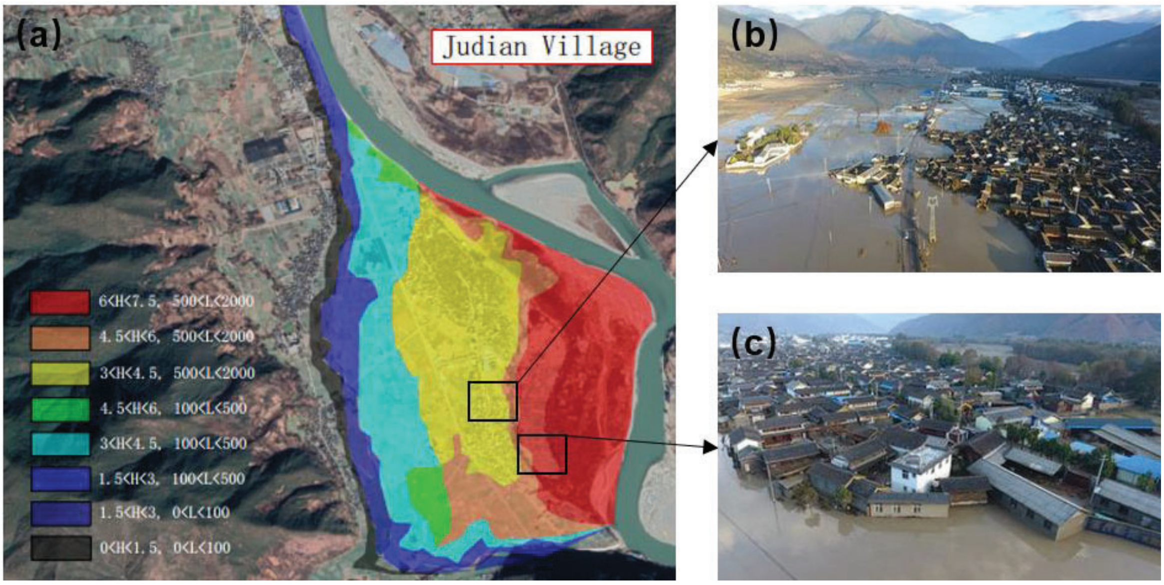

Fig. 11 The inundation area in Judian village caused by the breach of second Baige landslide dam: (a) risk zoning map; (b) and (c) inundation situation in real scenario (downstream view, cited from wap.eastday.com).

4.1. Human risk in Yulong County

The fatality ratio in Yulong County is calculated based on the parameters shown in Table 7 and the procedure discussed above. The human risk results are shown in Table 8. In Scenario 2, due to the long distance between the dam site and the towns downstream, the evacuation rate in the five towns is 99.99%, and only 2 people in Judian town may not be evacuated before the flood arrives. Despite a higher flood intensity and a greater water depth in Scenario 2, the fatality ratio is relatively low due to a high evacuation rate. No people lose their lives during the breach of the second landslide dam, while much farmland and many buildings have been inundated in Scenario 2.

The evacuation rates in the downstream towns for Scenario 3 are lower than those for Scenario 2, with values of 99.92% and 99.98% in Judian and Shigu towns, respectively, and 99.99% in Tacheng, Liming and Longpan. Seven people and 1 person in Judian and Shigu towns, respectively, may be in danger before the flood arrives. In addition, with a larger inundated area and significant water depth in Scenario 3, at least 4 people in Judian town and 1 person in Shigu town may lose their lives, while no people have to die in the other three towns due to the smaller inundated area.

A comparison of the results of Scenario 2 and 3 reveals that a diversion channel can significantly reduce the risk faced by people in downstream areas by lowering the dam height and the storage capacity of the barrier lake, and controlling the arrival time of the outburst flood.

Table 7 Inputs to eight basic nodes in five towns of Lijiang City. L is the evacuation distance, T is time of day, D_{dam} is the distance to dam site, B_{sn} is the building story number, T_b is dam breaching duration, H is the water depth, V is the flow velocity and B_y is the building type.

Scenario	Town	L (m)	T	D_{dam} (km)	B_{sn}	T_b (h)	H (m)	V (m/s)	B_y
	Tacheng	0-100		486			0-1.5	>6	
	Judian	0-2000		515			0-7.5	4-6	
S1	Liming	0-100	08:00-17:00	541	3	50	0-1.5	2-4	Concrete and brick
	Shigu	0-500		579			0-4.5	1-2	
	Longpan	0-100		614			0-1.5	1-2	
	Tacheng	0-100		486			0-6.0	>6	
	Judian	0-2000		515			0-11.0	4-6	
S2	Liming	0-100	08:00-17:00	541	3	45	0-4.5	4-6	Concrete and brick
	Shigu	0-500		579			0-9.0	1-2	
	Longpan	0-100		614			0-4.5	2-4	

Table 8 Fatality ratio and loss of life in five towns of Lijiang City.

Scenario	Town	At-risk population	Evacuation rate/%	Exposed population	Fatality ratio/%	Loss of life
S2	Tacheng	150	99.99	0	$6.58e^{-4}$	$9.87e^{-4}$
	Judian	6,341	99.98	2	$5.60e^{-3}$	$3.55e^{-1}$
	Liming	181	99.99	0	$1.30e^{-6}$	$2.35e^{-6}$
	Shigu	1,700	99.99	0	$1.62e^{-3}$	$2.77e^{-2}$
	Longpan	30	99.99	0	$7.30e^{-8}$	$2.19e^{-8}$
Sum	–	8,402	–	2	–	$3.84\ e^{-1}$
S3	Tacheng	450	99.99	0	$1.58e^{-3}$	$7.11e^{-3}$
	Judian	8,400	99.92	7	$4.20e^{-2}$	3.53
	Liming	452	99.99	0	$1.13e^{-3}$	$5.11e^{-3}$
	Shigu	3,345	99.98	1	$6.31e^{-3}$	$2.11e^{-1}$
	Longpan	92	99.99	0	$8.54e^{-4}$	$7.85e^{-4}$
Sum	–	12,739	–	8	–	3.75

5. Economic risk analysis

Economic risk can be divided into the following two parts: residential property loss (L_{RP}) and public property loss (L_{PP}). The former includes the movable and unmovable properties of local residents, while the loss of infrastructures and the evacuation cost are considered public property losses.

The residential property loss L_{RP} can be described as:

$$L_{RP} = L_{RM} + L_{RU} \tag{2}$$

where L_{RM} and L_{RU} are the moveable and unmovable residential property losses, respectively, which can be calculated as:

$$L_{RM} = (PAR)(I_N)n\alpha(1 - P_{eva}) \tag{3}$$

$$L_{RU} = (PAR)(I_N)n(1 - \alpha) \tag{4}$$

where PAR refers to the at-risk population, which is calculated by the ratio of the inundated area to the total residential area in each location; I_N is the rural residents' net annual income per person, with a value of RMB 4970, which is the average net income from 2003 to 2018 in the rural area of Yulong County (YMBS, 2004-2019); n is the average working period per person (20 years is assumed (Peng et al., 2013)); α is the proportion of movable properties and is set as 0.1 (Peng et al., 2013 and Shi et al., 2017); and P_{eva} is the evacuation rate calculated in the HURAM (Table 8).

The total public property loss consists of two parts: loss of infrastructure (L_I) and evacuation cost (L_C), and it can be expressed as follows:

$$L_{PP} = L_I + L_C \tag{5}$$

The loss of infrastructures is assumed to be uniformly distributed with the inundated area. Thus, the loss of infrastructures is estimated as:

$$L_I = \gamma A_S \tag{6}$$

where A_S refers to the total inundated area in each town, and γ refers to the total infrastructure property loss per unit area, which can be estimated as:

$$\gamma = \frac{P_T}{A_T} \tag{7}$$

where P_T and A_T refer to the loss of infrastructure and inundated area in each town, respectively. In Scenario 2, the total inundated area in Yulong County is 13.24 km^2 (Table 6), and the loss of infrastructure is RMB 3.48 billion Yuan, as reported by the local government. Thus, γ can be estimated by the total inundated area and loss of infrastructure in Yulong County as 0.263 billion yuan per km^2.

The evacuation cost can be divided into the following two parts: the expenses for evacuating and arranging the people at risk and necessary services and the GDP interruption (Peng and Zhang, 2013a):

$$L_C = L_{ci} + L_{GDP} \tag{8}$$

$$L_{ci} = \mathrm{c}P_{eva}(PAR)(w_t + 3) \tag{9}$$

$$L_{GDP} = \frac{GDP_p}{365}(PAR)(w_t + 4) \tag{10}$$

where c refers to the expense per person per day (60 yuan), w_t is the period from the issuance of warning to the arrival of flood (5 days), and GDP_p is the average GDP per person in the flood area, which is 28,764 yuan (YMBS, 2019).

5.1. Economic risk in Yulong County

The economic risk in Yulong County for Scenarios 2 and 3 is shown in Table 9. Both the residential property loss and the public property loss in Scenario 3 increase significantly, with values 51.66% and 32.43% higher than that in Scenario 2, respectively. In the residential property loss, the movable residential property loss for Scenario 2 and 3 can be ignored due to the high evacuation rate in the downstream area. In the public property loss, the evacuation cost is relatively small comparing to the infrastructure loss, which is less than 1% of the total public property loss in both Scenario 2 and 3. However, the growth of evacuation cost between the two scenarios is larger than that of infrastructure loss (50% and 32.38%, respectively), due to the larger inundation area which is induced by the flood of Scenario 3.

The total loss of property in Scenario 2 evaluated by the methods mentioned above is 4.24 billion yuan, which is very close to the loss of property reported by the local government (4.20 billion yuan). The total loss of property in Scenario 3 is 5.757 billion yuan, which is 35.84%

higher than that in Scenario 2 and is also much higher than the cost of disposing of the landslide dam by excavating a diversion channel. these results indicate that a diversion channel excavated on the dam crest can significantly decrease the loss of property downstream by attenuating the flood intensity, and it is an efficient way to address such an emergency event.

Table 9 Loss of property in five towns of Yulong County. L_{RP} and L_{PP} is the residential and public property loss respectively, L_{RM} is the movable residential property loss, L_{RU} is the unmovable residential property loss, L_I is the loss of infrastructures and L_C is the evacuation cost.

Scenario	Town	L_{RP} (Billion)			L_{PP} (Billion)		
		L_{RM}	L_{RU}	L_{RP}	L_I	L_C	L_{PP}
S2	Tacheng	$1.49e^{-7}$	0.01	0.01	0.22	$1.78e^{-4}$	0.22
	Judian	$1.26e^{-5}$	0.57	0.57	1.82	0.01	1.83
	Liming	$1.80e^{-7}$	0.02	0.02	0.27	$2.15e^{-4}$	0.27
	Shigu	$1.69e^{-6}$	0.15	0.15	0.93	0.00	0.93
	Longpan	$2.98e^{-8}$	0.00	0.00	0.24	$3.56e^{-5}$	0.24
Sum		$1.47e^{-5}$	0.75	0.75	3.48	0.01	3.49
S3	Tacheng	$4.47e^{-7}$	0.04	0.04	0.34	$5.35e^{-4}$	0.34
	Judian	$6.68e^{-5}$	0.75	0.75	2.27	0.01	2.28
	Liming	$4.49e^{-7}$	0.04	0.04	0.38	$5.37e^{-4}$	0.38
	Shigu	$6.65e^{-6}$	0.30	0.30	1.29	0.01	1.30
	Longpan	$9.15e^{-8}$	0.01	0.01	0.31	$1.09e^{-4}$	0.31
Sum		$7.44e^{-5}$	1.14	1.14	4.59	0.02	4.61

6. Discussion

Normally, there is a long-time lag between co-site landslide dams' formation. In these cases, the relationship between them can be neglected. However, the two Baige landslide dams formed at the same site and breached within a month, leading to a close relationship between the dam's geometry, flood routing and risks. In this circumstance, although the volume of the second landslide is much smaller than that of the first one, the second dam height was much higher than usual and the second lake volume was larger too, resulting in an amplification effect of the flood intensity and downstream risks.

The amplification effect that exists between the two landslide dams is attributed to the existence of the residual dam with a non-negligible height, the fragmentation and entrainment effect. A residual dam can significantly increase the resulting dam height and lake volume. The volume of water released by the landslide dams breach thus increases due to the existence of residual dam, leading to an increase in the peak outflow rate and risks in downstream locations. Since the rock mass of the second landslide dam was fine and loose, it was highly vulnerable to erosion. Under these circumstances, it appears necessary to take relevant emergency mitigation measures to dispose of the residual dam, in order to reduce the amplification effect between the two landslide dams and to lower the risk faced by people and property downstream. In fact, a third potential landslide that may fail in the future was monitored at the same place (Ouyang et al., 2019), and the residual deposits of the second landslide dam were removed to reduce the influence of the residual dam (Fig. 1A).

6.1. Diversion channel

This section aims to propose an optimal design for the diversion channel. Assuming a trapezoidal shape for the diversion channel, the peak outflow rate (Q_p) during the breach of a landslide dam is a function of:

$$Q_p = Q_p(W_b, D, S, G_s, V) \tag{11}$$

in which W_b, D, S and G_s are the bottom width, depth, side slope and longitudinal gradient of the diversion channel, respectively (Fig. 12). V is the excavation volume of the diversion channel, and it can be calculated by the other four geometric parameters as follows:

$$\mathrm{V} = \int_{-\frac{D}{tanB_u+G_s}}^{0} (2W_b + 2\frac{D_u}{tanS})\frac{1}{2}D_u dx + \int_0^L (2W_b + 2\frac{D_m}{tanS})\frac{1}{2}D_m dx + \int_L^{L+\frac{G_sL+D}{tanB_d-G_s}} (2W_b + 2\frac{D_d}{tanS})\frac{1}{2}D_d dx \tag{12}$$

where B_u and B_d are the slope angles of the dam upstream and downstream, respectively. L is the top width of the dam. D_u, D_m, and D_d are the depths of the diversion channel in L_1, L_2 and L_3, respectively, and can be expressed as:

$$D_u = D + x(tanB_u + G_s) \tag{13}$$

$$D_m = D + xG_s \tag{14}$$

$$D_d = D + G_s L + (L - x)(tanB_d - G_s) \tag{15}$$

In order to obtain the optimal design of the diversion channel, the following conditions concerning the five parameters in Equation (11) are considered. The excavation volume of the diversion channel is set as a constant number (here 44,704 m^3) to ensure the same cost in excavating the diversion channel, regardless of its shape. Parameter S is set as less than 38° to ensure the stability of the side slope, L is 79.4 m, and W_b, D and G_s are greater than 0. Thus, the function of Q_p can be rewritten as:

$$Q_p = Q_p(W_b, D, S, G_s)|_{(V\leq 44703, S\leq 38°, W_b>0, D>0, G_s>0)} \tag{16}$$

Based on Equation (16), the DABA model, which is developed by Chang and Zhang (2010) to simulate the outflow curve as well as the breach, is used to calculate the peak outflow rate with different geometric parameters of the diversion channel satisfying conditions (16).

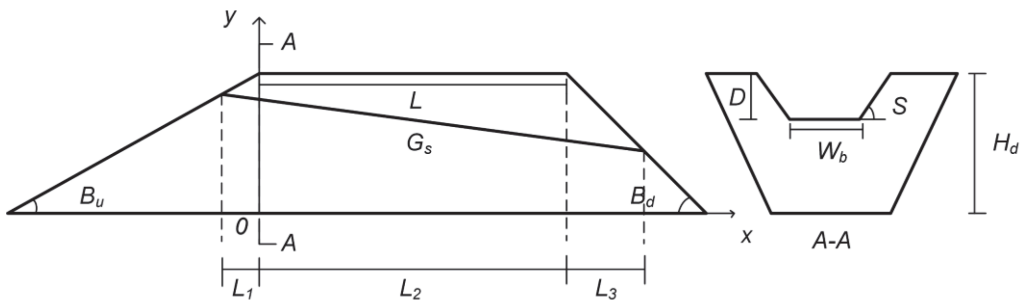

Fig. 12 A sketch map of diversion channel

The influence of the depth and bottom width of the diversion channel on the peak outflow rate is shown in Fig. 13a, where G_s is constant (0.006), as considered in the real case. As shown in Fig. 13a, the peak outflow rate decreases with increasing depth. This is because the lake capacity decreases significantly with increasing depth of the diversion channel, leading to a smaller peak outflow rate at the dam site. The peak outflow rate also decreases with increasing bottom width, while the reduction rate is much smaller. This is because the diversion channel with a narrow bottom width must have a small side slope angle, and further leading to the small erosion rate of dam materials and higher peak outflow rate at the dam site (Chang and Zhang

2010; Zhu et al., 2021). The results also indicate that a diversion channel with a deep and narrow cross-section is better at reducing the peak outflow rate, and the depth is the main factor that influence the peak outflow rate. The results show little difference if the variation of longitudinal gradient of the diversion channel is considered (Fig. 13b). Under the same depth of the diversion channel, the peak outflow rate first decreases with increasing longitudinal gradient and then increases. This is because a larger gradient can significantly increase the water erosional competency at the formation phase of the dam breach if the dam width is relatively large, leading to a flatter outflow rate curve and a smaller peak outflow rate. However, if the situation of the second Baige landslide dam is considered, with a relatively small width, and relatively large depth and longitudinal gradient of the diversion channel, the coarser materials with lower erodibility at the bottom of the dam may be exposed to the dam break flood. This portion of the material is difficult to wash away by flooding, leading to a much steeper outflow rate curve with a relatively large peak outflow rate.

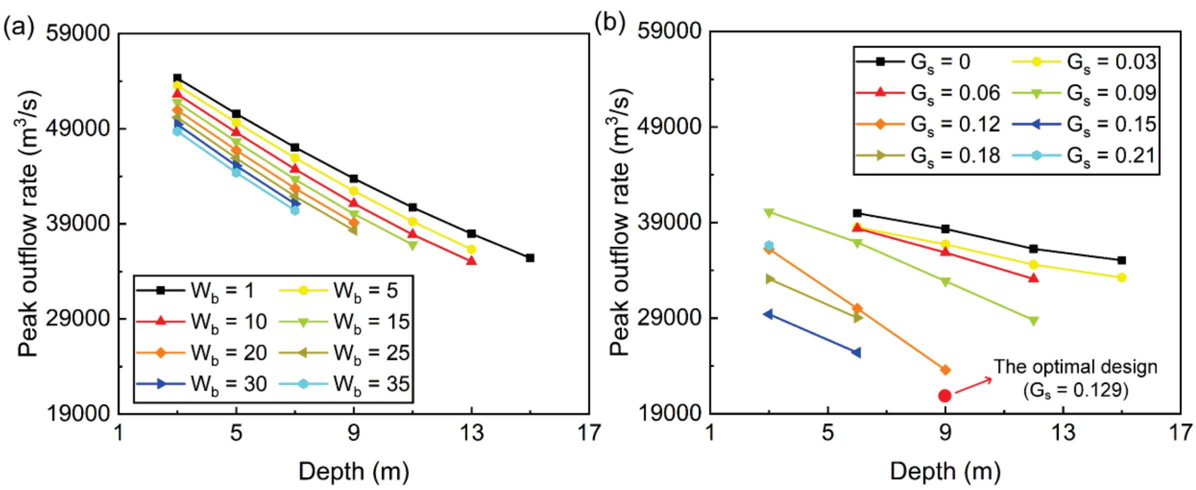

Fig. 13 Relationship between peak outflow rate and the geometry parameters of the diversion channel.

Furthermore, based on the relationship between the peak outflow rate and the geometric parameters of the diversion channel, the smallest peak outflow rate of Q_p=19,767 m^3/s can be accessed for a diversion channel with D=9 m, W_b=3 m, S=38° and G_s=0.129. The peak outflow rate is reduced by 41.69% compared to that in Scenario 2 (19,767 m^3/s vs. 33,900 m^3/s).

The flood routing results are shown in Table 10. Compared to the large decrease of the peak outflow rate at the dam site, the changes of the peak outflow rate in the downstream towns are not obvious. In addition, the variation in the maximum water level in the downstream towns is so small that the discrepancy can be ignored, which means that the inundation area downstream with the optimal diversion channel is almost equal to that in Scenario 2.

Table 10 Flood routing results in five towns of Yulong County. S_{OD} refers to the scenario of optimal diversion channel design, Q_p and W_{dm} represent the peak outflow rate and the maximum water depth respectively.

Town	S_{OD}		S2		Reduction rate ($S2-S_{OD}/S2$)	
	Q_p (m^3/s)	W_{dm} (m)	Q_p (m^3/s)	W_{dm} (m)	Q_p	W_{dm}
Tacheng	13,218	1.53	13,386	1.52	0.01	-0.01
Judian	12,078	7.93	11,873	7.47	-0.02	-0.06
Liming	11,879	1.72	11,552	1.49	-0.03	-0.15
Shigu	9,586	5.32	8,844	4.52	-0.08	-0.18
Longpan	7,223	1.25	6,543	0.56	-0.10	-1.23

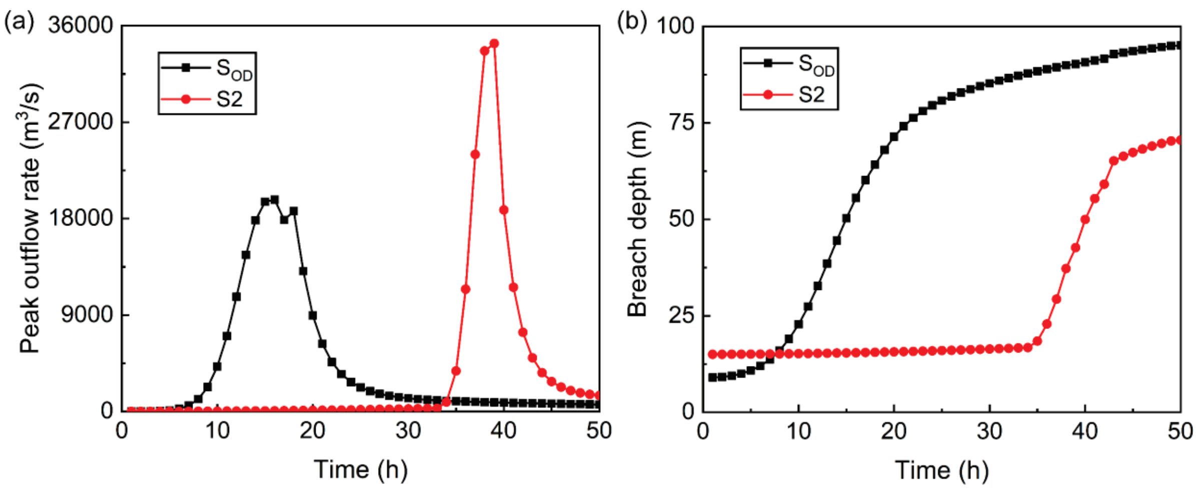

Fig. 14 The comparation between S2 and S_{OD} (scenario of optimal diversion channel design) (a) comparation of peak outflow rate curve; (b) comparation of breach depth.

The variation in the peak outflow rate and maximum water depth between the dam site and downstream towns is attributed to the attenuation of the peak outflow rate along the river. Lininger and Latrubesse (2016) suggested that the attenuation of the peak outflow rate is influenced by four kinds of parameters, including the storage areas, roughness of the river channel and floodplain, geometric characteristics and hydrology. In the 2018 Baige case, the outflow rate curve in the optimal case is flatter than that in Scenario 2 (Fig. 14a). Due to the slow energy dissipation, this flatter-shaped outflow rate curve needs a longer time and distance to attenuate the peak outflow rate to a relatively small value than the steeper curve, even though the peak outflow rate is relatively small (Yang et al., 2020). With little difference of flood intensity between the two scenarios, risks faced by people and property downstream do not change, and the efficiency of the optimal diversion channel is almost equal to that in Scenario 2. However, another advantage occurs when the optimal diversion channel is considered. As shown in Fig. 14b, a larger breach depth occurs in the optimal case, which indicates an increased efficiency in dredging the river channel for the use of the optimal diversion channel. Furthermore, as the Baige landslide dams' site may be blocked by another landslide event in the future, the amplification effect may be reduced in the case of the optimal diversion channel.

7. Conclusion

The flood intensity and economic risk caused by the breach of the second Baige landslide dam (Scenario 2) increase significantly compared to those resulting from the failure of the first dam (Scenario 1). The major reasons are the existence of the first residual dam and the higher erodibility of dam materials. The residual dam increases the second dam height and lake volume, and the more erodible dam materials make the surface erosion much faster. However, the expected loss of life in S1 and S2 are small because of the sufficient time lag provided by the long distance between the residential area and the dam site.

Diversion channels are effective ways to reduce the peak outflow rate and risks downstream. Without the diversion channel (Scenario 3), the expected loss of life would be 3.75, and the economic loss would be 1.52 billion yuan higher than that in Scenario 2, which is much higher than the cost of excavating a diversion channel.

The depth and longitudinal gradient of the diversion channel significantly influence the peak outflow rate. The peak outflow rate decreases significantly with increasing depth, while it first decreases and then increases with increasing the longitudinal gradient of the diversion channel due to the influence of the erodibility of the dam materials and the relatively small dam width. The peak outflow rate can be further decreased by considering the optimal diversion channel with a depth of 9 m and a longitudinal gradient of 0.129.

The peak outflow rate in the downstream towns does not change with consideration of optimal diversion channel. A relatively small attenuation rate of the peak outflow rate occurs with a flatter outflow rate curve due to its slow energy dissipation. However, the amplification effect for a potential co-site landslide dam in the future may be reduced since the residual dam height is highly reduced by the optimal diversion channel.

This study provides a scientific basis for the risk mitigation of co-site landslide dams, and the methods mentioned in this paper can be used in risk control and decision-making of landslide dams in the future.

Acknowledgments

The authors acknowledge the support from the Natural Science Foundation of China (No. 41731283, No.42071010, No.4201101075 and No. 41877234), and the Shanghai Natural Science Foundation (No.20ZR1461300).

Appendix

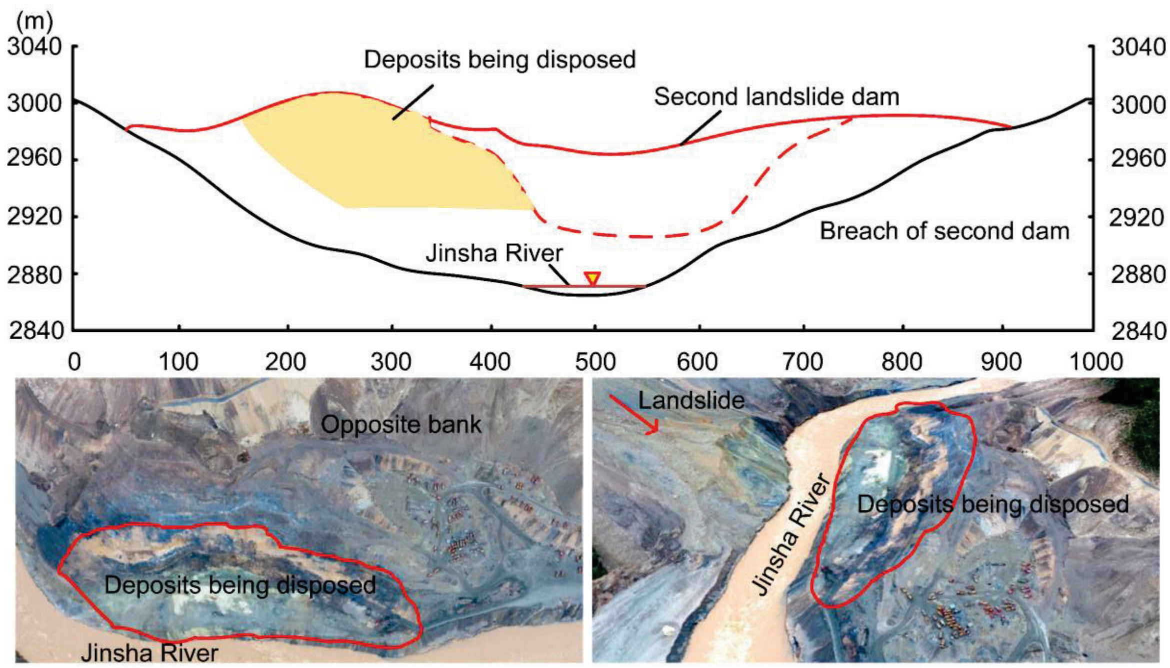

Fig. 1A Deposits that have been removed

Reference

Chang, D., Zhang, L., 2010. Simulation of the erosion process of landslide dams due to overtopping considering variations in soil erodibility along depth. Natural Hazards and Earth System Sciences, 10(4), 933.

Chen, X., Cui, P., You, Y., Cheng, Z., Khan, A., Ye, C., Zhang, S., 2017. Dam-break risk analysis of the Attabad landslide dam in Pakistan and emergency countermeasures. Landslides 14:675-683.

Cui, P., Dang, C., Zhuang, J., You, Y., Chen, X., and Kevin, M. S. 2010. Landslide-dammed lake at Tangjiashan, Sichuan province, China (triggered by the Wenchuan Earthquake, May 12, 2008): Risk assessment, mitigation strategy, and lessons learned. Environ Earth Sci, 65:1055–1065.

Ermini, L., Casagli, N., 2003. Prediction of the behavior of landslide dams using a geomorphological dimensionless index. Earth Surface Processes&Landforms 28(1):31-47.

Fan, X., Zhan, W., Dong, X., Westen, C., Xu, Q., Dai, L., Yang, Q., Huang, R.Q., Havenith, H.B., 2018. Analyzing successive landslide dam formation by different triggering mechanism: The case of the Tangjiawan landslide, Sichuan, China. Engineering Geology 243:128-144.

Fan, X., Xu, Q., Andres, A., Srikrishnan, S.S., Li, W., Zheng, G., Dong, X., Huang, R., 2019. Successive landsliding ad damming of the Jinsha River in eastern Tibet, China: Prime investigation, early warning, and emergency response. Landslides 16:1003-1020.

Frey, H., Huggei, C., Chisolm, R.E., Baer, P., McArdell, B., Cochachin, A., Portocarrero, C., 2018. Multi-source glacial lake outburst flood hazard assessment and mapping for Huaraz, Cordillera Blanca, Peru. Frontiers in Earth Science 6:210.

Hydrologic Engineering Centre (HEC), 2008. HEC-RAS, River analysis system, hydraulic reference manual, version 4.0, developed by Hydrologic Engineering Centre of US Army Corps of Engineers, Washington.

Li, Y., Fan, X, Cheng, G., 2006. Landslide and rockfall distribution by reservoir of stepped hydropower station in the Jinsha River. Wuhan University Journal of Natural Sciences, 11(4), 801-805.

Liao, H., Yang, X., Xu, F., Xu, H., Zhou, J., 2018. A fuzzy comprehensive method for the risk assessment of a landslide-dammed lake. Environmental Earth Sciences 77:750.

Lininger, K.B., Latrubesse, E.M., 2016. Flooding hydrology and peak discharge attenuation along the middle Araguaia River in central Brazil, Catena 143: 90-101.

Ouyang, C., An, H., Zhou, S., Wang, Z., Su, P., Wang, D., Cheng, D., She, J., 2019. Insights from the failure and dynamic characteristics of two sequential landslides at Baige village along the Jinsha River, China. Landslides 16(7):1397-1414.

Peng, M., Ma, C., Chen, H., Zhang, P., Zhang, L., Jiang, M., Zhang, Q., Shi, Z., 2021. Experimental study on breaching mechanisms of landslide dams composed of different materials under surge waves. Engineering Geology, 291, 106242.

Peng, M., Zhang, L.M., 2012a. Breaching parameters of landslide dams. Landslides 9(1):13-31.

Peng, M., Zhang, L., 2012b. Analysis of human risks due to dam break floods - Part 1: A new model based on bayesian networks. Natural Hazards and Earth System Sciences 64(1):903-933.

Peng, M., Zhang, L., 2013a. Dynamic decision making for dam-break emergency management – Part 1: Theoretical framework. Natural Hazards and Earth System Sciences 13: 425-437.

Peng, M., Zhang, L., Chang, D., Shi, Z., 2014 Engineering risk mitigation measures for the landslide dams induced by the 2008 Wenchuan earthquake. Engineering Geology 180:68-

84.
Shang, Y., Yang, Z., Li, L., Liu, D., Liao, Q., Wang, Y., 2003. A super-large landslide in Tibet in 2000: Background, occurrence, disaster, and origin. Geomorphology 54:225-243.
Shen, D., Shi, Z., Peng, M., Zhang, L., Jiang, M., 2020. Longevity analysis of landslide dams. Landslides 17(8): 1797-1821.
Shi, Z., Xiong, X., Peng, M., Zhang, L., Xiong, Y., Chen, H., Zhu, Y., 2017. Risk assessment and mitigation for the hongshiyan landslide dam triggered by the 2014 Ludian Earthquake in Yunnan, China. Landslides 14(1):1-18.
Tang, C., Hu, J., Lin, M., Angelier, J., Lu, C., Chan, Y., Chu, H., 2009. The Tsaoling landslide triggered by the Chi-Chi earthquake, Taiwan: Insights from a discrete element simulation. Engineering Geology 106:1-19.
Wang, S., and Liu, J., 2013. Modeling the risk assessment of landslide-dammed lakes based on the emergency response measures in Wenchuan earthquake, 2008, China. Natural hazards 67(2): 523-547.
Xiong, Z., Feng, G., Feng, Z., Miao, L., Wang, Y., Yang, D., Luo, S., 2020. Pre-and post-failure spatial-temporal deformation pattern of the Baige landslide retrieved from multiple radar and optical satellite images. Engineering Geology, 279, 105880.
Xu, F., Yang, X., Zhou, J., 2017. Dam-break flood risk assessment and mitigation measures for the Hongshiyan landslide-dammed lake triggered by the 2014 Ludian earthquake. Geomatics, Natural Hazards and Risk 8(2):803-821.
Yang, Q., Guan, M., Peng, Y., Chen, H., 2020. Numerical investigation of flash flood dynamics due to cascading failures of natural landslide dams. Engineering Geology, 276, 105765.
Yang, S., Pan, Y., Dong, J., Yeh, K. C., and Liao J., 2013. A systematic approach for the assessment of flooding hazard and risk associated with a landslide dam. Natural Hazards, 65, 41-62.

Yunnan Municipal Burean of Statistics (YMBS), 2004-2019. Statistical bulletin for national economic and social development of Yunnan Province. stats.yn.gov.cn. online: http://stats.yn.gov.cn/tjsj/tjnj/201901/t20190121_834593.html. (in Chinese).

Zhang, L., Xiao, T., He, J., Chen, C., 2019. Erosion-based analysis of breaching of Baige landslide dams on the Jinsha River, China, in 2018. Landslides 16:1965-1979.

Zhang, X., Xue, R., Wang, M., Yu, Z., Li, B., Wang, B., 2020. Field investigation and analysis on flood disasters due to Baige landslide dam break in Jinsha River, Advanced Engineering Sciences 52(5): 89-100.

Zhu, X., Liu, B., Peng, J., Zhang, Z., Zhuang, J., Huang, W., Leng, Y., Duan, Z., 2021. Experimental study on the longitudinal evolution of the overtopping breaching of noncohesive landslide dams. Engineering Geology, 288, 106137.